Theory for polymer analysis using nanopore-based single-molecule mass spectrometry

Joseph E. Reiner[1], John J. Kasianowicz, Brian J. Nablo, and Joseph W. F. Robertson[1]

Semiconductor Electronics Division, Electronics and Electrical Engineering Laboratory, National Institute of Standards and Technology, 100 Bureau Drive, Gaithersburg, MD 20899-8120

Edited by Nicholas J. Turro, Columbia University, New York, NY, and approved June 1, 2010 (received for review February 25, 2010)

Nanometer-scale pores have demonstrated potential for the electrical detection, quantification, and characterization of molecules for biomedical applications and the chemical analysis of polymers. Despite extensive research in the nanopore sensing field, there is a paucity of theoretical models that incorporate the interactions between chemicals (i.e., solute, solvent, analyte, and nanopore). Here, we develop a model that simultaneously describes both the current blockade depth and residence times caused by individual poly(ethylene glycol) (PEG) molecules in a single α-hemolysin ion channel. Modeling polymer-cation binding leads to a description of two significant effects: a reduction in the mobile cation concentration inside the pore and an increase in the affinity between the polymer and the pore. The model was used to estimate the free energy of formation for K^+-PEG inside the nanopore (≈ − 49.7 meV) and the free energy of PEG partitioning into the nanopore (≈0.76 meV per ethylene glycol monomer). The results suggest that rational, physical models for the analysis of analyte-nanopore interactions will develop the full potential of nanopore-based sensing for chemical and biological applications.

alpha-hemolysin | nanopore-based sensing | polymer confinement | polymer analysis

Polymers play a fundamental role in life (1) and are central to many emerging technologies (2). Many of these applications require a detailed understanding of the structure, morphology, and chemical interactions of polymers under confinement in either 2-dimensional films (3) or narrow tubes (4). The ability to isolate and study single molecules has shown promise in overcoming the limitations of measurements with ensemble averages and permits probing the inter- and intra-molecular forces, structural changes, and dynamics of polymers (for a detailed review of single-molecule polymer analysis see refs. 5 and 6).

Molecules partition into a nanopore and alter the flow of ions resulting in distinct current blockades that can be used to detect, characterize, and quantify a wide range of polymer types (7). These include single-stranded RNA and DNA (8–10), proteins (11–14), biowarfare agents (15), therapeutic agents against anthrax toxins (15, 16), and chemically synthesized molecules (14, 17–20). More recently, single nanopores were used to determine the size distribution of polymers in a manner akin to mass spectrometry (19).

To fully realize the potential of nanopore-based sensors, it is important to develop a detailed understanding of the physical and chemical interactions of polymers with the nanopore, solvent, electrolyte, and other components. In this work, the interaction between poly(ethylene glycol) (PEG) and the α-hemolysin (αHL) channel in a high ionic strength electrolyte was used to develop a unique model of polymers confined within single nanopores.

Previous attempts to describe the magnitude of PEG-induced nanopore current blockades focused on volume exclusion (21) and/or microviscosity (22), which required adjustable ad hoc parameters with no clear physical basis, to fit the data. The residence time of the polymer in the pore, which contains information about chemical interactions, was associated with an unrelated model (22, 23). These studies were further limited because the effect of polydispersity was either not observed directly (22) or noted but ignored in the analysis (23). Here, we describe a physical model that accounts for both the current blockades and residence times, caused by a wide range of PEG sizes, with a single thermodynamic picture. The model assumes that polymer volume exclusion and the binding of ions to the polymer leads to a reduction in the single channel current and an enhancement in PEG binding to the pore. This predictive capability is based on chemical interactions between the analyte, nanopore, and electrolyte, which provides previously undescribed insights into single-molecule characterization with a nanopore sensor.

Results

Individual molecules of PEG are detected and characterized by monitoring the change in the ionic current caused by the partitioning of the polymer in a single αHL channel (19). In the absence of analyte, the current through the channel is stable, with no observed gating events, and has a time-averaged value, $\langle i_o \rangle$ (19, 22, 24, 25). PEG partitions into the channel causing the current to decrease (17, 19, 21, 22, 26, 27). When PEG is added to the *trans* side of the membrane, the current blockades are sufficiently long to analyze with a thresholding algorithm from which a time-averaged current $\langle i \rangle$ for each blockade event is determined (Fig. 1 *A* and *B*; see *SI Text* for details). Notably, the blockade signals caused by nonelectrolyte PEGs show a decrease in both the mean time between blockades and the average blockade duration for an increase in the magnitude of the applied potential (Fig. 1*C*). Electroosmotic flow does not cause the latter effect because the slightly anion selective nature of the αHL causes a net solvent flow through the pore that is opposite that of the applied electric field (25, 28–30). This would lead to a decrease in the PEG capture rate with increasing electric field.

It is more likely that PEG, which is known to coordinate cations (31–35), behaves like a polycation in a high ionic strength solution. This explains the observed increase in the PEG blockade frequency with increasing (negative) electric field (23). Here, we describe the PEG-αHL interaction with a simple physical and chemical model based on first-order cation-PEG binding kinetics, which results in a charged molecule fixed in a nanopore. This model describes the voltage dependencies of both the residence time and blockade depth as PEG interacts with the pore and establishes a link between them.

Author contributions: J.E.R., J.J.K., and J.W.F.R. designed research; B.J.N. and J.W.F.R. performed research; J.E.R. contributed new reagents/analytic tools; J.E.R. and J.W.F.R. analyzed data; J.E.R., J.J.K., and J.W.F.R. developed the model; and J.E.R., J.J.K., and J.W.F.R. wrote the paper.

Conflict of interest statement: J.W.F.R. and J.J.K. have filed a provisional patent for single-molecule sizing with a nanopore. J.E.R., J.J.K., and J.W.F.R. are filing a provisional patent for aspects of the work in this manuscript.

This article is a PNAS Direct Submission.

Freely available online through the PNAS open access option.

[1]To whom correspondence may be addressed. E-mail: joseph.reiner@nist.gov or joseph.robertson@nist.gov.

This article contains supporting information online at www.pnas.org/lookup/suppl/doi:10.1073/pnas.1002194107/-/DCSupplemental.

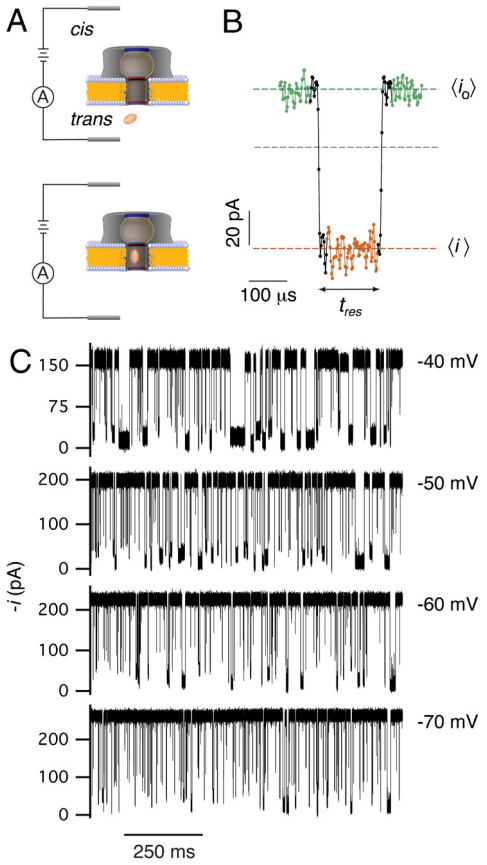

Fig. 1. PEG causes transient current blockades in a single α-hemolysin nanopore. (*A*) PEG reversibly partitions into and out of the pore causing well-defined current blockades. (*B*) A thresholding algorithm is used to detect the events. The blockade amplitude is defined by averaging the open channel current immediately adjacent to the event, $\langle i_o \rangle$ (green points), and the base of the blockade, $\langle i \rangle$ (orange points). The black data points represent transition states and are not used in the analysis. The residence time (t_{res}) is the difference between the onset and the termination of the event. (*C*) Current traces show that increasing the magnitude of the applied transmembrane voltage increases the frequency of blockade events and decreases blockade lifetimes. The *trans* solution contained a mixture of PEG with approximately equimolar concentrations of mean molecular masses M_w = 1,000 g/mol, 1,500 g/mol, 2,000 g/mol, and 3,000 g/mol and a chemically purified internal standard of PEG M_w = 1,294 g/mol in 4 M KCl, 10 mM tris adjusted to pH 7.5 with citric acid.

The relative frequency distribution of the PEG blockade events, $\langle i \rangle / \langle i_o \rangle$, reduces to sharp peaks that clearly separate individual n-mers of the polymer, where n is the degree of polymerization (Fig. 2). In a previous study, a sample of PEG M_w = 1,500 g/mol was analyzed with the αHL channel and calibrated with a chemically purified PEG external standard (19). In this work, the $\langle i \rangle / \langle i_o \rangle$ distribution was observed over a much wider range of polymer sizes from a mixture of PEG with mean molecular masses M_w = 3,000 g/mol, 2,000 g/mol, 1,500 g/mol, and 1,000 g/mol and an internal standard of purified PEG M_w = 1,294 g/mol, (i.e., $n = 29$). As observed previously (19), the mixture produced many peaks with four significantly overlapping distributions (Fig. 2). Unexpectedly, the mean peak conductance values shifted to higher values as the potential was increased.

Due to the high resolution achieved in the data shown here, the residence time distribution for each n-mer was readily accessible. The probability density of each residence time was characterized by a single exponential function with a mean residence time, $\langle \tau_n \rangle$, for all n-mers ($18 < n < 70$) within the potential range investigated (-40 mV $< V_{app} < -70$ mV) (see *SI Text* for details). For the 30-mer, as the potential was decreased from −40 mV to −70 mV, $\langle \tau_n \rangle$ decreased by nearly 100-fold (Fig. 3). A similar strong voltage-dependence was obtained for all the polymer sizes studied herein. These results strongly suggest that the polymer-nanopore system can be described with a simple first-order kinetic reaction model, discussed in detail below.

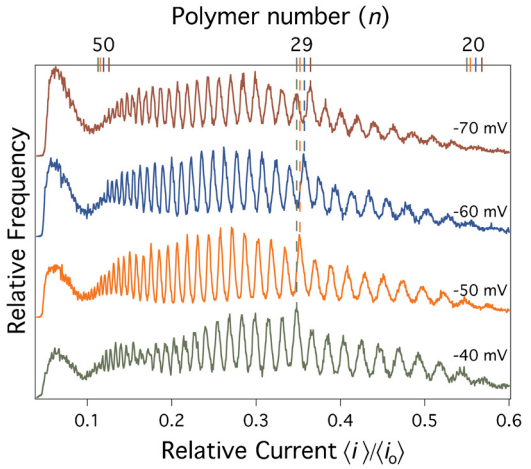

Fig. 2. PEG-induced single channel current reduction distributions are voltage-dependent. Increasing the applied potential decreased the normalized current blockade amplitude. This effect is described by a model in which cations bind to PEG molecules (Eq. **5**). The color-coded tick marks above the peaks for polymer n-mers with n = 20, 29 and 50 illustrate typical voltage-dependent shifts over a range of polymer size. The tick color corresponds to the magnitude of the voltage (green: −40 mV, orange: −50 mV, blue: −60 mV, and red: −70 mV). The shift was observed for all resolved peaks. Each distribution was formed with >130,000 blockade events.

Theory

We propose a simple model where PEG decreases the ionic current by reducing the concentration of mobile ions in the pore through two mechanisms: volume exclusion and cation complexation with the polymer. The latter decreases the local diffusion coefficient of ions in the pore in a manner similar to fixed proton buffers (36). Including the cation binding to PEG leads to a description of PEG-induced current blockades with explicit dependence on the applied potential and cation concentration.

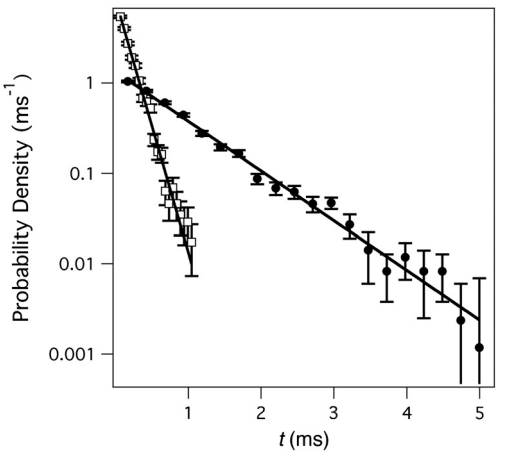

Fig. 3. The residence time distribution for a given size PEG n-mer in the nanopore is exponential and voltage-dependent. The solid lines are least squares fits of $P(t) = A \exp(-t/\langle \tau_n \rangle)$ to the data for a PEG molecule of size $n = 30$, $V_{app} = -70$ mV, $\langle \tau_{30} \rangle = (0.154 \langle \pm \rangle 0.03)$ms (open squares) and $V_{app} = -40$ mV, $\langle \tau_{30} \rangle = (0.78 \langle \pm \rangle 0.01)$ms (solid circles). Similar results were obtained for all the polymers characterized here and all values of the applied potential.

Current Blockades. ***Confinement of PEG in the αHL pore.*** Consider the αHL nanopore to be a right circular cylinder with length L_{pore} and cross-sectional area A_{pore} (29, 37). For a 1:1 electrolyte solution, the Nernst–Planck equation describes the ionic current density along the axial coordinate, z,

$$J_{\pm,z}(\vec{r}) = -\frac{e^2}{k_{\text{B}}T}\tilde{C}_{\pm}(\vec{r})\tilde{D}_{\pm}(\vec{r})\frac{\partial V(\vec{r})}{\partial z} \mp |e|\tilde{D}_{\pm}(\vec{r})\frac{\partial \tilde{C}_{\pm}(\vec{r})}{\partial z} \quad [1]$$

where $J_{\pm,z}$ are the cation (+) and anion (−) steady-state current densities along the z-axis, e is the electron charge, k_{B} is Boltzmann's constant, T is the absolute temperature, $\tilde{C}_{\pm}$ are the spatially varying mobile ion concentration profiles, $\tilde{D}_{\pm}$ are the spatially varying diffusion coefficient profiles, and V is the electrical potential within the nanopore. Combining Eq. **1** with the Poisson equation for the electrical potential leads to a complete description of the current through the nanopore. Numerical simulations for these Poisson–Nernst–Planck (PNP) equations were performed for αHL alone to estimate the electric field distribution in the pore and to understand the channel's weak anion selectivity (29).

Despite the complexity suggested by PNP simulations, the salient features of the PEG-induced current blockade data are well described with a few simplifying assumptions. First, the pore is partitioned into five regions: The PEG bound to the pore wall defines L_{PEG}, the PEG-free regions of the pore on either end of the polymer, and the two boundary regions (see *SI Text*). The current in each region of the nanopore is the sum of contributions from both anions and cations integrated over the cross-sectional area of the pore, i.e., $\langle i\rangle = \iint_{\text{pore}} dxdy(J_{+,z}(x,y) + J_{-,z}(x,y))$. Assuming the voltage dependence along the length of the nanopore is piecewise linear and that the steady-state current in each region is the same leads to the following expression for the relative change in the current upon partitioning of a PEG molecule into the pore (see *SI Text* for a detailed derivation)

$$\frac{\langle i\rangle}{\langle i_o\rangle} = \left(1 - \frac{L_{\text{PEG}}}{L_{\text{pore}}}(1-y)\right)^{-1}, \quad [2]$$

where y is given by

$$y = \frac{2C_oD_oA_{\text{pore}}}{(A_{\text{pore}} - A_{\text{PEG}})(C_+D_+^{\text{eff}} + C_-D_-^{\text{eff}})}. \quad [3]$$

The polymer extends along the nanopore z-axis as estimated by $L_{\text{PEG}} = an^{\nu}$ (38) where $a = 1.45$ Å (39) is the effective monomer size and ν is a polymer size scaling parameter analogous to the Flory exponent (40). The density of PEG is assumed to be independent of mass so that the volume of each PEG molecule is $V_{\text{PEG}} = abn$ with the average cross-sectional area of the PEG, $A_{\text{PEG}} = bn^{1-\nu}$, where $b = 46.5$ Å^2 estimated from the specific gravity of PEG, $\rho = 1.08$ g/cm^3. The diffusion coefficient and concentration of both cations and anions in the PEG-free regions of the pore are assumed constant and equal to D_o and C_o, respectively. In the PEG occupied region of the pore these parameters ($\tilde{D}_{\pm}^{(P)}$ and $\tilde{C}_{\pm}^{(P)}$) are assumed to be independent of z and defined as fluctuations about the respective mean values $\tilde{C}_{\pm}^{(P)}(x,y) = C_{\pm} + \delta C_{\pm}(x,y)$ and $\tilde{D}_{\pm}^{(P)}(x,y) = D_{\pm} + \delta D_{\pm}(x,y)$. These expressions lead to an effective diffusion coefficient for anions and cations in the PEG occupied region of the pore $D_{\pm}^{\text{eff}}$

$$D_{\pm}^{\text{eff}} = D_{\pm} + \iint_{\text{pore}} dxdy\frac{\delta C_{\pm}(x,y)\delta D_{\pm}(x,y)}{(A_{\text{pore}} - A_{\text{PEG}})C_{\pm}}. \quad [4]$$

Under certain conditions (i.e., larger nanopores), the Debye–Hückel approximation can be used to estimate $D_{\pm}^{\text{eff}}$. Here, the integral is not evaluated explicitly (41, 42), but $D_{\pm}^{\text{eff}}$ is treated as part of two freely adjustable parameters (see below). Numerical simulations could provide a more precise estimation of $D_{\pm}^{\text{eff}}$ (43), but this is beyond the scope of the present manuscript.

Cation-PEG interactions. In this model, PEG reduces the current in two ways. First, the number of ions in the channel is reduced because of the volume excluded by the PEG. Second, cation binding to the PEG molecule further reduces the concentration of mobile cations in the PEG occupied region. The binding of m_b cations to the PEG follows a simple equilibrium reaction depicted schematically in Fig. 4 and is described by a first-order kinetic process, with an association constant (31, 44)

$$K_A = \frac{m_b}{(m_T - m_b)(nx - m_b)} = \exp(-\beta(\Delta G_{o,\text{pore}} + s^+e|V_{\text{app}}|)), \quad [5]$$

where $m_T = C_oL_{\text{PEG}}(A_{\text{pore}} - A_{\text{PEG}})$ is the total number of cations in the PEG occupied region, $1/x$ is the average number of monomers required to bind a single cation, $\beta = 1/(k_{\text{b}}T)$, $\Delta G_{o,\text{pore}}$ is the change in free energy upon binding a single cation to the PEG within the nanopore, V_{app} is the applied transmembrane potential, $s^+ = \gamma(1 - F_V^+/F_E^+)$ where γ defines the PEG position in the nanopore ($\gamma = 0.5$ for PEG at the center of the nanopore) (45), and F_V^+/F_E^+ is the ratio of the electroosmotically induced viscous force to the applied electric force on a single cation (41, 42, 46, 47). Assuming K_A is independent of m_b leads to the following expression for the average number of cations bound to the polymer,

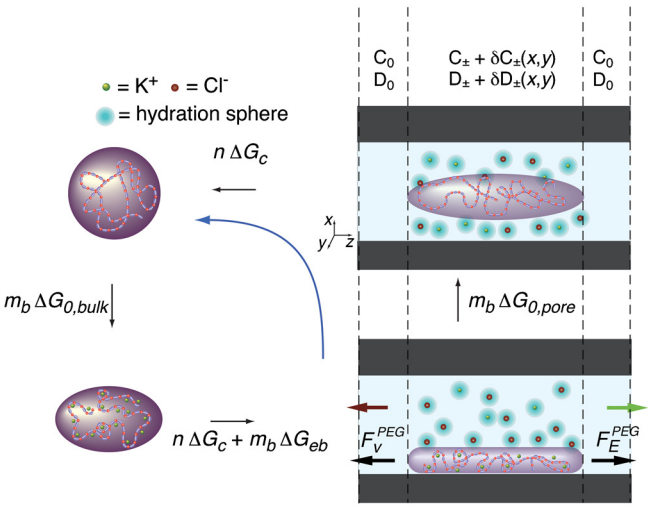

Fig. 4. The reaction scheme for the PEG, cation and nanopore interactions is described by two net reversible reactions: PEG-cation coordination and PEG-nanopore partitioning. In this simplified scheme m_b cations bind to a PEG n-mer with a free energy change of $m_b\Delta G_{o,\text{bulk}}$. The cation-PEG complex enters and binds to the pore, with confinement term, $n\Delta G_c$ (22, 23, 38), and a cation-associated binding term, $m_b\Delta G_{eb}$. The adsorption of the PEG-cation complex to the nanopore wall causes electroosmotic flow via the anions (for simplicity the boundary regions are neglected see *SI Text*). The arrows indicate the direction of flow for anions (red), cations (green), the applied electric force (F_E^{PEG}), and viscous force (F_V^{PEG}) on the entire PEG molecule. When m_b bound cations dissociate from the complex with a corresponding change in free energy, $m_b\Delta G_{o,\text{pore}}$, PEG exits the nanopore with a change in free energy $n\Delta G_c$. The total change in the free energy resulting from the exodus of PEG from the nanopore, used in Eq. **8**, comes from the combination of the two steps highlighted by the blue arrow.

$$m_b = \frac{\alpha - \sqrt{\alpha^2 - 4m_T nx}}{2} \quad [6]$$

where $\alpha = m_T + nx + K_A^{-1}$.

The mobile cation concentration is reduced by the PEG binding such that $C_+/C_o = 1 - m_b/m_T$ while the mobile anion concentration is unaffected by the binding so that $C/C_o = 1$. Thus, Eq. **3** can be rewritten as

$$y = \frac{2}{(a^* - b^* \frac{m_b}{m_T})(1 - \frac{A_{\text{PEG}}}{A_{\text{pore}}})} \quad [7]$$

where $a^* = (D_+^{\text{eff}} + D_-^{\text{eff}})/D_o$ and $b^* = D_+^{\text{eff}}/D_o$ are adjustable parameters. Substituting Eq. **6** into Eq. **7** and Eq. **7** into Eq. **2** leads to an expression for the PEG-induced current reduction. The model explicitly depends on both the applied voltage and the bulk cation concentration (Eq. **2**). The voltage dependence arises from the reduction of the barrier for ions to dissociate from the PEG complex and contribute to the current, which leads to the voltage dependence of the PEG-induced current reduction observed in Fig. **2**.

Residence Times. As has been shown experimentally, the residence time distributions for single polymers confined in a nanopore are characteristic of the polymer type. Polymers with fixed charges, such as single-stranded nucleic acids (8, 37, 48) or poly(styrene sulfonate) (18), have residence time distributions that are either peaked (i.e., Gaussian-like) with relatively high applied potentials or exponential with small applied potentials. For example, Talaga and Li estimated the probability distribution of protein translocation through a solid-state nanopore with a first passage time model based on one-dimensional diffusion of the polymers through a uniform electric field (49). In that case the theoretical residence time distributions are skewed Gaussians, which are consistent with their data. Conversely, several studies hypothesized that exponentially distributed blockades are caused by charged polymers that do not traverse the membrane (18, 47, 50). For our experiments, the residence times for a given size PEG are exponentially distributed regardless of polymer size or value of the applied potential.

The free energy of dissociation of PEG from the nanopore determines the mean PEG residence times. Our model assumes the PEG binding to the nanopore is described by a multistep process where cation association with the polymer causes a conformational change in the latter, which leads to an enhanced PEG binding to the nanopore. If this enhanced binding ΔG_{eb} is much stronger than $\Delta G_{o,\text{pore}}$, and the enhanced binding only occurs when a cation is bound to the PEG, then the resulting change in the free energy of PEG dissociating from the nanopore can be approximated by $\Delta G_{\text{bind}} = m_b \Delta G_{o,\text{pore}} + n\Delta G_c$ (see Fig. 4*D*), where ΔG_c is the free energy of confining the uncharged polymer per monomer. If the free and activation energies of dissociation are equal, then the mean PEG blockade residence time can be estimated using the Arrenhius rate equation

$$\langle \tau_n \rangle = \tau_o \exp(-\beta(n\Delta G_c + m_b(\Delta G_{o,\text{pore}} + s^{\text{PEG}} e|V_{\text{app}}|))) \quad [8]$$

where τ_o is the nonbinding diffusion limited residence time of the polymer in the pore and $s^{\text{PEG}} = \gamma(1 - F_V^{\text{PEG}}/F_E^{\text{PEG}})$ where $F_V^{\text{PEG}}/F_E^{\text{PEG}}$ is the ratio of the electroosmotically induced viscous force to the applied electric force on the entire PEG molecule.

In the absence of PEG binding with the nanopore, the polymer complex moves in the nanopore at a constant drift velocity, v_{PEG}, so that $\tau_o = L_{\text{pore}}/v_{\text{PEG}}$. v_{PEG} can be estimated by balancing the force from the applied electric field on the entire PEG molecule, $F_E^{\text{PEG}} = em_b V_{\text{app}}/L_{\text{pore}}$, with F_V^{PEG} and the hydrodynamic drag force F_S. For a cylinder in an infinite solution with viscosity, η, F_S can be approximated to first order in $\varepsilon = (\ln(\sqrt{\pi} L_{\text{PEG}}/\sqrt{A_{\text{PEG}}}))^{-1}$ as $F_S = 2\pi\eta\varepsilon L_{\text{PEG}} v_{\text{PEG}}$ (51), which leads to the following expression for τ_o

$$\tau_o = \frac{\xi\varepsilon L_{\text{PEG}}}{m_b|V_{\text{app}}|} \quad [9]$$

where $\xi = 2\pi\eta B L_{\text{pore}}^2/(e(1 - F_V^{\text{PEG}}/F_E^{\text{PEG}}))$ and B is the ratio of the PEG terminal velocity in an infinite medium and the terminal velocity of the polymer confined in a cylinder. B depends on $A_{\text{PEG}}/A_{\text{pore}}$ in a nontrivial way, which can only be estimated numerically (52). Here, it is part of the free parameter ξ.

Interestingly, there is a link between the current blockade depth and the mean PEG residence time through the parameters m_b and $\Delta G_{o,\text{pore}}$ (Eq. **8**). Specifically, the cation-PEG interaction alters both the reduction in current and also causes an enhanced binding of the PEG to the nanopore, which in turn affects the duration of the current blockade. This PEG-cation binding model accounts for previous observations of PEG residence times and current blockades in the αHL channel (19, 21–23) and includes explicit dependencies on the applied potential.

Estimation of Parameters. The model relies on adjustable parameters that have clear physical meaning. The blockade depth (Eq. **2**) depends on the free energy of cation-polymer adsorption within the nanopore, $\Delta G_{o,\text{pore}}$, the bulk electrolyte concentration C_o, the mean number of bonds formed between the cation and polymer $1/x$, the polymer length scaling exponent, ν, the effective ion diffusion coefficients within the vicinity of the PEG $D_\pm^{\text{eff}}$, the PEG binding location within the nanopore γ, and the ratio of the forces from the applied electric field to the anion induced electroosmotic flow on a single cation F_V^+/F_E^+. The expression for the residence time (Eq. **8**) includes the free energy of confinement, ΔG_c, the ratio of the forces from the applied electric field to the anion induced electroosmotic counter flow on the entire PEG molecule, $F_V^{\text{PEG}}/F_E^{\text{PEG}}$, and the hydrodynamic drag term, ξ. To reduce the number of freely adjustable parameters, C_o/N_A, where N_A is Avogadro's number, is set equal to the molar concentration in the bulk solution (4 M), $\nu = 0.6$, the polymer behaves as if it were in a good solvent, $L_{\text{pore}} = 49.5$ Å and $A_{\text{pore}} = 450$ Å^2 (53). The blockade amplitude and residence time dependencies on n were simultaneously fit using the global analysis algorithm in Motofit (54). The result of the fit to the blockade depth data at $V_{\text{app}} = -50$ mV is shown in Fig. 5*A* with residuals for each applied potential in Fig. 5*C* (for the full datasets see *SI Text*); the result of the residence time fit is shown in Fig. 5*D* with the normalized residuals in Fig. 5*E*. In total, eight parameters were adjusted to fit eight sets of data consisting of at least 30 points each. The parameters are estimated to be (±1 S.D.) $1/x = 4.83 \pm 0.03$, $\Delta G_{o,\text{pore}} = -(49.7 \pm 0.5)$ meV, $\Delta G_c = (0.76 \pm 0.09)$ meV, $s^+ = 0.21 \pm 0.01$, $s^{\text{PEG}} = 0.14 \pm 0.01$, $\xi = (7.6 \pm 0.2)$ Vs/m, $a^* = 1.22 \pm 0.02$, and $b^* = 1.14 \pm 0.02$. The global reduced chi-square value is $\chi^2 = 1.3$.

Discussion

This study presents a previously undescribed technique for investigating equilibrium chemistry on a single-molecule level. The estimated parameters compare favorably with existing numerical and experimental studies. The best-fit value for $1/x$ suggests that on average approximately five monomers bind a single cation, which is consistent with PEG's ability to chelate potassium ions (31). Reported values for PEG-K^+ binding in vacuum (44) are an order of magnitude larger than the $\Delta G_{o,\text{pore}}$ estimated here. This discrepancy is likely due to two reasons: The vacuum measurements do not account for solvation energies of either ions or polymer in the nanopore environment, and our model neglects the effect of repulsive cation-cation interactions, which would decrease the apparent binding energy. More detailed numerical

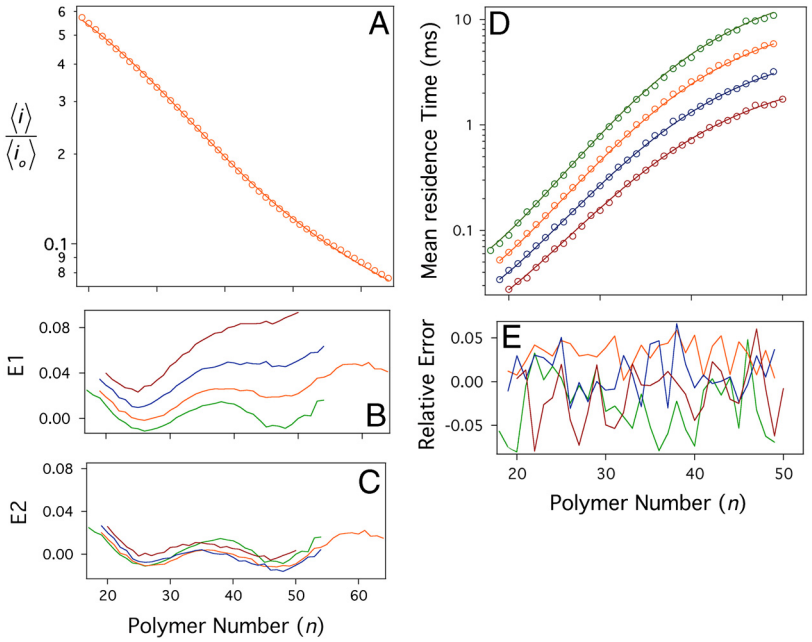

Fig. 5. Mean current blockade amplitudes and polymer residence times as a function of polymer size and applied potential were simultaneously fit by the chemical reaction model. (*A*) Experimentally determined current blockade amplitudes (open orange circles) and least-squares fits from the model defined in Eq. **2** (solid orange line) for data obtained at $V_{app} = -50$ mV. See *SI Text* for the full dataset. (*B*) The normalized residuals ($E1 = 1 - \frac{\langle i \rangle}{\langle i_o \rangle}|_{\frac{-40\text{ mV}}{\text{MODEL}}} / \frac{\langle i \rangle}{\langle i_o \rangle}|_{\text{DATA}}$) calculated from current blockades measured at four different applied potentials [−40 mV (green), −50 mV (orange), −60 mV (blue), and −70 mV (red)], but with V_{app} held fixed at −40 mV in Eq. **2**, show the explicit voltage dependence of the blockade amplitudes. (*C*) However, when the actual voltages are used in the model, the normalized residuals converge ($E2 = 1 - \frac{\langle i \rangle}{\langle i_o \rangle}|_{\text{MODEL}} / \frac{\langle i \rangle}{\langle i_o \rangle}|_{\text{DATA}}$). (*D*) Experimentally determined PEG residence times in the nanopore (open circles) and least-squares fits from Eq. **8** (solid lines) along with normalized residuals above. The data and fits correspond to V_{app} values of −40 mV (green), −50 mV (orange), −60 mV (blue), and −70 mV (red) for each plot. (*E*) Normalized residuals between the residence time data and model (Eq. **8**).

analysis of cation binding within the nanopore may resolve this difference. In addition to the energetics of the interaction between cations and polymers, the model also suggests that the polymer must overcome a confinement barrier of $\approx$ 0.76 meV/monomer to enter the nanopore. This is a significant departure from previous treatments, which suggest that there is a decrease in free energy upon PEG confinement with an entropic penalty only paid when the polymer volume exceeds the pore volume (22, 23). Although the confinement free energy per monomer is relatively weak, the total free energy of confinement becomes larger than k_BT at room temperature for $n > 32$. Clearly, one can not ignore the free energy penalty paid for any polymer under confinement.

Binding cations to PEG and fixing the charged complex within a nanopore induces electroosmotic flow counter to the applied electric field. This leads to a viscous force that reduces the net force acting on the PEG molecule. For double-stranded DNA held in place with an optical tweezer in a larger ($r \geq 5$ nm) nanopore, continuum hydrodynamic equations along with the Debye–Hückel approximation were used to calculate $F_V/F_E \sim 0.5$ (41, 42, 46, 47). Of course, these assumptions fail for the αHL nanopore due to the breakdown of the continuum equations for electrostatics in such a confined geometry (41). Nevertheless, here we estimate $F_V^{\text{PEG}}/F_E^{\text{PEG}}$ by assuming the PEG molecule resides in the center of the nanopore ($\gamma = 0.5$) and from the best-fit value of s^{PEG} we find $F_V^{\text{PEG}}/F_E^{\text{PEG}} = 0.72 \pm 0.02$, which is in reasonable agreement with the values obtained for the DNA-solid state nanopore system (41, 42, 46). This value for $F_V^{\text{PEG}}/F_E^{\text{PEG}}$, $\xi = 7.6$ Vs/m and $\eta = 0.001$ Ns/m^2 for the bulk viscosity of water leads to $B = 2.2$, which implies that the terminal velocity inside the nanopore is just under half its value in bulk solution (52). Finally, the best-fit values for a^* and b^* imply $D_+^{\text{eff}}/D_o = 1.14$ and $D_-^{\text{eff}}/D_o = 0.08$, which is consistent with Eq. **4** and three physically reasonable assumptions, $\delta C_+ \approx -\delta C_-$ (46), and the mobility of the cations and anions is similar (54) so that $\delta D_+ \approx \delta D_-$ and $D_+ \approx D_-$.

Our theoretical model for the interactions between cations, PEG, and the αHL channel is in excellent agreement with our high-resolution PEG-induced current reduction and residence time data (Fig. 5 *A* and *D*, respectively). However, the normalized residuals of the current blockade oscillate with an error larger than the standard error of the measurement, which suggests the model does not fully account for all the details. It is conceivable that this oscillation provides a key to the microscopic picture of how PEG binds to cations by coiling around the ions in order to maximize the number of ion-dipole bonds formed. This could in principle also give rise to an improved environment for hydrogen bonding between the polymer-cation complex and the many hydroxyl residues on the interior of the β-barrel of αHL. A more complete picture of this enhanced PEG-nanopore binding could be developed through molecular dynamics simulations (MD) (47). Additional improvement could be achieved with a more thorough description of the actual electrostatic potential profile within the nanopore through 3-D PNP simulations (37, 43, 56–59). Nevertheless, our simple theoretical model captures the essence of the experimental results and suggests that cations play a significant role in creating an environment for polymers to interact with the nanopore, providing an explanation for why the residence time for PEG is so long (i.e., $\geq 10^3$-fold longer than expected), providing the theoretical basis for single-molecule mass spectrometry in a nanopore. The development of a physicochemical model for the interactions between ions, polymers, and a nanopore improves the likelihood for nanoporous sensors to be used to size (akin to mass spectrometry) and chemically differentiate between a wide range of biological molecules (e.g., DNA, RNA, and proteins) and synthetic polymers.

Materials and Methods

Solvent-free planar lipid membranes were formed from DPhyPC (1,2 diphytanolyl-*sn*-glycero-3-phosphatidylcholine; Avanti Polar Lipids, Alabaster, AL) in *n*-decane (Sigma-Aldrich, St Louis), on either quartz or borosilicate glass capillaries prepared as described by White and colleagues (60–62). The glass pores used for this study had diameters that ranged between 1.1 μm and 1.5 μm. The capillary was filled with a mixture of poly(ethylene glycol) (PEG) at 9 mg/mL $M_w = 1000$ g/mol, 13.4 mg/mL $M_w = 1500$ g/mol, 18 mg/mL $M_w = 2000$ g/mol, 28 mg/mL $M_w = 3000$, and 2 mg/mL of chemically purified PEG $M_w = 1294$ g/mol all in 4 M KCl (Sigma-Aldrich, St. Louis), 10 mM tris (Schwarz/Mann Biotech, Cleveland) at pH 7.2, titrated with saturated citric acid (Fluka, Buchs, Switzerland). The solution external to the capillary was the same 4 M KCl solution, but without polymer. Membranes were formed by first treating the glass with 0.4 μL of a 0.1% v/v solution of hexadecane in pentane (Aldrich). The solution bath external to the glass capillary was coated with 0.6 μL to 1.2 μL of DPhyPC dissolved in a 10 mg/mL mixture in *n*-decane. After ≈2 min, the solution level was raised above the pore, spontaneously forming a membrane.

Single channel measurements were obtained by allowing a single α-hemolysin channel to self-assemble into the membrane by injecting 0.4 μL to 0.6 μL

of a 0.5 mg/mL solution of α-hemolysin in pH 7.2 buffer (List Biological Laboratories, Campbell, CA) and applying a slight back pressure (≈80 mm Hg to 110 mm Hg) from the capillary side to thin the membrane. After a single channel formed, the pressure was reduced to ≈20 mm Hg to prevent further channel insertion and formation.

Additional methods can be found in *SI Text*.

ACKNOWLEDGMENTS. Henry White provided helpful instructions for working with conical glass pores and generously donated glass nanopore supports.

We thank Electronic Biosciences, LLC, for building a high-impedance amplifier and data acquisition system for our laboratory under a National Institute of Standards and Technology (NIST) Small Business Innovation Research grant. This work was sponsored in part by grants from the NIST Office of Law Enforcement Standards and NIST Office of Microelectronics Projects. Certain commercial equipment, instruments, or materials are identified in this work to specify the experimental procedure adequately. Such identification is not intended to imply recommendation or endorsement by NIST, nor is it intended to imply that the materials or equipment identified are necessarily the best available for this purpose.

1. Di Marzio E (2002) Profound implications for biophysics of the polymer threading a membrane transition. *Structure and Dynamics of Confined Polymers*, eds JJ Kasianowicz, MSZ Kellermayer, and DW Deamer (Kluwer, Dordrecht, The Netherlands), Vol 87, pp 1–22.
2. Forrest S (2004) The path to ubiquitous and low-cost organic electronic appliances on plastic. *Nature* 428:911–918.
3. Granick S, et al. (2003) Macromolecules at surfaces: Research challenges and opportunities from tribology to biology. *J Polym Sci Pol Phys* 41:2755–2793.
4. Gay C, deGennes P, Raphaël E, Brochard-Wyart F (1996) Injection threshold for a statistically branched polymer inside a nanopore. *Macromolecules* 29:8379–8382.
5. Barbara PF, Chang W, Link S, Scholes GD, Yethiraj A (2007) Structure and dynamics of conjugated polymers in liquid crystalline solvents. *Ann Rev Phys Chem* 58:565–584.
6. Deniz AA, et al. (2001) Ratiometric single-molecule studies of freely diffusing biomolecules. *Annu Rev Phys Chem* 52:233–253.
7. Kasianowicz JJ, Robertson JWF, Chan ER, Reiner JE, Stanford VM (2008) Nanoscopic porous sensors. *Annu Rev Anal Chem* 1:737–766.
8. Kasianowicz JJ, Brandin E, Branton D, Deamer DW (1996) Characterization of individual polynucleotide molecules using a membrane channel. *Proc Natl Acad Sci USA* 93:13770–13773.
9. Akeson M, Branton D, Kasianowicz JJ, Brandin E, Deamer DW (1999) Microsecond time-scale discrimination among polycytidylic acid, polyadenylic acid, and polyuridylic acid as homopolymers or as segments within single RNA molecules. *Biophys J* 77:3227–3233.
10. Vercoutere W, et al. (2001) Rapid discrimination among individual DNA hairpin molecules at single-nucleotide resolution using an ion channel. *Nat Biotechnol* 19:248–252.
11. Movileanu L, Schmittschmitt JP, Scholtz JM, Bayley H (2005) Interactions of peptides with a protein pore. *Biophys J* 89:1030–1045.
12. Oukhaled G, et al. (2007) Unfolding of proteins and long transient conformations detected by single nanopore recording. *Phys Rev Lett* 98:158101.
13. Goodrich CP, et al. (2007) Single-molecule electrophoresis of beta-hairpin peptides by electrical recordings and Langevin dynamics simulations. *J Phys Chem B* 111:3332–3335.
14. Oukhaled G, Bacri L, Mathe J, Pelta J, Auvray L (2008) Effect of screening on the transport of polyelectrolytes through nanopores. *Europhys Lett* 82:48003.
15. Halverson K, et al. (2005) Anthrax biosensor, protective antigen ion channel asymmetric blockade. *J Biol Chem* 280:34056–34062.
16. Karginov VA, et al. (2006) Search for cyclodextrin-based inhibitors of anthrax toxins: Synthesis, structural features, and relative activities. *Antimicrob Agents Ch* 50:3740–3753.
17. Movileanu L, Bayley H (2001) Partitioning of a polymer into a nanoscopic protein pore obeys a simple scaling law. *Proc Natl Acad Sci USA* 98:10137–10141.
18. Murphy RJ, Muthukumar M (2007) Threading synthetic polyelectrolytes through protein pores. *J Chem Phys* 126:051101.
19. Robertson JWF, et al. (2007) Single-molecule mass spectrometry in solution using a solitary nanopore. *Proc Natl Acad Sci USA* 104:8207–8211.
20. Gibrat G, et al. (2008) Polyelectrolyte entry and transport through an asymmetric alpha-Hemolysin channel. *J Phys Chem B* 112:14687–14691.
21. Bezrukov SM, Vodyanoy I, Brutyan RA, Kasianowicz JJ (1996) Dynamics and free energy of polymers partitioning into a nanoscale pore. *Macromolecules* 29:8517–8522.
22. Krasilnikov OV, Rodrigues CG, Bezrukov SM (2006) Single polymer molecules in a protein nanopore in the limit of a strong polymer-pore attraction. *Phys Rev Lett* 97:018301.
23. Rodrigues CG, Machado DC, Chevtchenko SF, Krasilnikov OV (2008) Mechanism of KCl enhancement in detection of nonionic polymers by nanopore sensors. *Biophys J* 95:5186–5192.
24. Bezrukov SM, Kasianowicz JJ (1993) Current noise reveals protonation kinetics and number of ionizable sites in an open protein ion channel. *Phys Rev Lett* 70:2352–2355.
25. Kasianowicz JJ, Bezrukov SM (1995) Protonation dynamics of the alpha-toxin ion-channel from spectral-analysis of pH dependent current fluctuations. *Biophys J* 69:94–105.
26. Krasilnikov O, Sabirov R, Ternovsky V, Merzliak P, Muratkhodjaev J (1992) A simple method for the determination of the pore radius of ion channels in planar lipid bilayer-membranes. *FEMS Microbiol Immun* 105:93–100.
27. Krasilnikov OV (2002) Sizing channels with neutral polymerss. *Structure and Dynamics of Confined Polymers*, eds JJ Kasianowicz, MSZ Kellermayer, and DW Deamer (Kluwer, Dordrecht, The Netherlands), Vol 87, pp 97–116.
28. Merzlyak PG, Capistrano MFP, Valeva A, Kasianowicz JJ, Krasilnikov OV (2005) Conductance and ion selectivity of a mesoscopic protein nanopore probed with cysteine scanning mutagenesis. *Biophys J* 89:3059–3070.
29. Noskov SY, Im W, Roux B (2004) Ion permeation through the α-hemolysin channel: Theoretical studies based on Brownian Dynamics and Poisson–Nernst–Plank electrodiffusion theory. *Biophys J* 87:2299–2309.
30. O'Keeffe J, Cozmuta I, Bose D, Stolc V (2007) A predictive MD–Nernst–Planck model for transport in alpha-hemolysin: Modeling anisotropic ion currents. *Chem Phys* 342:25–32.
31. Tasaki K (1999) Poly(oxyethylene)-cation interactions in aqueous solution: a molecular dynamics study. *Comput Theor Polym S* 9:271–284.
32. Hakem IF, Lal J (2002) Evidence of solvent-dependent complexation in non-ionic polymer-salt systems. *Appl Phys A-Mater* 74:S531–S533.
33. Heeb R, Lee S, Venkataraman N, Spencer N (2009) Influence of salt on the aqueous lubrication properties of end-grafted, ethylene glycol-based self-assembled monolayers. *ACS Appl Mater Interfaces* 1:1105–1112.
34. Liu K-J (1968) Nuclear magnetic resonance studies of polymer solutions. V. Cooperative effects in the ion-dipole interaction between potassium iodide and poly(ethlene oxide). *Macromolecules* 1:308–311.
35. Park JH, et al. (2008) Influence of salts on ionic diffusion in oligomer electrolytes and its implication in dye-sensitized solar cells. *J Photoch Photobio A* 194:148–151.
36. Junge W, McLaughlin S (1987) The role of fixed and mobile buffers in the kinetics of proton movement. *Biochim Biophys Acta* 890:1–5.
37. Aksimentiev A, Schulten K (2005) Imaging alpha-hemolysin with molecular dynamics: Ionic conductance, osmotic permeability, and the electrostatic potential map. *Biophys J* 88:3745–3761.
38. deGennes P (1979) *Scaling Concepts in Polymer Physics* (Cornell Univ Press, Ithaca, NY).
39. Lee H, Venable RM, MacKerell AD, Pastor RW (2008) Molecular dynamics studies of polyethylene oxide and polyethylene glycol: Hydrodynamic radius and shape anisotropy. *Biophys J* 95:1590–1599.
40. Flory P (1949) The configuration of real polymer chains. *J Chem Phys* 17:303–310.
41. Ghosal S (2007) Effect of salt concentration on the electrophoretic speed of a polyelectrolyte through a nanopore. *Phys Rev Lett* 98:238104.
42. Ghosal S (2007) Electrokinetic-flow-induced viscous drag on a tethered DNA inside a nanopore. *Phys Rev E* 76:061916.
43. Coalson R, Kurnikova M (2005) Poisson–Nernst–Planck theory approach to the calculation of current through biological ion channels. *IEEE T Nanobiosci* 4:81–93.
44. More MB, Ray D, Armentrout PB (1997) Cation-ether complexes in the gas phase: Bond dissociation energies of K^+(dimethyl ether)$_x$, $x = 1$–4; K^+(1,2-dimethoxyethane)$_x$, $x = 1$ and 2; and K^+(12-crown-4). *J Phys Chem A* 101:4254–4262.
45. Woodhull A (1973) Ionic blockage of sodium channels in nerve. *J Gen Physiol* 61:687–708.
46. van Dorp S, Keyser UF, Dekker NH, Dekker C, Lemay SG (2009) Origin of the electrophoretic force on DNA in solid-state nanopores. *Nat Phys* 5:347–351.
47. Luan B, Aksimentiev A (2008) Electro-osmotic screening of the DNA charge in a nanopore. *Phys Rev E* 78:021912.
48. Lubensky DK, Nelson DR (1999) Driven polymer translocation through a narrow pore. *Biophys J* 77:1824–1838.
49. Talaga DS, Li J (2009) Single-molecule protein unfolding in solid state nanopores. *J Am Chem Soc* 131:9287–9297.
50. Forrey C, Muthukumar M (2007) Langevin dynamics simulations of ds-DNA translocation through synthetic nanopores. *J Chem Phys* 127:015102.
51. Ui T, Hussey R, Roger R (1984) Stokes drag on a cylinder in axial motion. *Phys Fluids* 27:787–795.
52. Brizard M, Megharfi M, Mahe E, Verdier C (2005) Design of a high precision falling-ball viscometer. *Rev Sci Instrum* 76:025109.
53. Song LZ, et al. (1996) Structure of staphylococcal alpha-hemolysin, a heptameric transmembrane pore. *Science* 274:1859–1866.
54. Nelson A (2006) Co-refinement of multiple-contrast neutron/X-ray reflectivity data using MOTOFIT. *J Appl Crystallogr* 39:273–276.
55. MacInnes D (1961) *The Principles of Electrochemistry* (Dover, New York).
56. Barcilon V, Chen D, Eisenberg R (1992) Ion flow through narrow membrane channels. 2. *SIAM J Appl Math* 52:1405–1425.
57. Cardenas A, Coalson R, Kurnikova M (2000) Three-dimensional Poisson–Nernst–Planck theory studies: Influence of membrane electrostatics on gramicidin A channel conductance. *Biophys J* 79:80–93.
58. Chen D, Eisenberg R (1993) Flux, coupling, and selectivity in ionic channels of one conformation. *Biophys J* 65:727–746.
59. Muthukumar M, Kong CY (2006) Simulation of polymer translocation through protein channels. *Proc Natl Acad Sci USA* 103:5273–5278.
60. Ervin EN, White RJ, White HS (2009) Sensitivity and signal complexity as a function of the number of ion channels in a stochastic sensor. *Anal Chem* 81:533–537.
61. White RJ, et al. (2007) Single ion-channel recordings using glass nanopore membranes. *J Am Chem Soc* 129:11766–11775.
62. White RJ, et al. (2006) Ionic conductivity of the aqueous layer separating a lipid bilayer membrane and a glass support. *Langmuir* 22:10777–10783.